Covert ISAC Against Collusive Wardens

Yujie Wu, Chengwen Xing, *Member, IEEE,* Jie Tang, *Senior Member, IEEE,* Nan Zhao, *Senior Member, IEEE,* Xiu Yin Zhang, *Fellow, IEEE,* Kai-Kit Wong, *Fellow, IEEE,* and George K. Karagiannidis, *Fellow, IEEE*

***Abstract*—Integrated sensing and communication (ISAC) is seen as a future solution to frequency congestion due to its excellent ability to simultaneously support target sensing and information transmission. To guarantee robust data security and privacy protection, covert communication can be employed in ISAC systems. In this paper, we propose a covert ISAC scheme against collusive wardens. In particular, a dual-function base station transmits the sensing beamforming to continuously sense an aerial target while communicating with a ground receiver with a probability of 0.5 via the communication beamforming. First, we derive a closed-form expression of the detection outage probability of each warden to obtain the global detection outage probability. Under the worst case that the wardens can collusively adjust their detection thresholds to achieve the best detection performance, we jointly optimize the communication and sensing beamformings to maximize the covert transmission rate. To tackle this non-convex problem, unitary-iteration and zero-forcing schemes are proposed to transform it into convex ones via semidefinite relaxation and successive convex approximation, respectively. Numerical results demonstrate the validity of the proposed covert ISAC scheme, which can achieve a better trade-off among communication, sensing and covertness compared to benchmarks.**

***Index Terms*—Integrated sensing and communication, covert communication, collusive wardens, beamforming optimization, covert transmission rate.**

I. Introduction

With the rapid development of mobile networks, the communication and radar devices are proliferating, putting tremendous pressure on the limited spectrum resource [2]. Integrated sensing and communication (ISAC) emerges as a promising technology to address this issue due to its particular ability to realize the communication and sensing services on a unified hardware platform simultaneously, and allow the communication and radar systems to share the same spectrum resource [3]–[5]. Compared with traditional communication and radar systems, ISAC can offer significant benefits of low cost, low power, and small volume via sharing the hardware circuits [6]. In addition, due to the similar signal processing architecture for both the communication and sensing, ISAC can design flexible waveforms to allow the selection of communication-centric [7], sensing-centric [8], and co-designed [9] ones according to the multifarious communication and sensing requirements. Due to its high compatibility, ISAC can be combined with a variety of advanced techniques to enhance performance including non-orthogonal multiple access (NOMA), intelligent reflecting surface (IRS), unmanned aerial vehicle (UAV), and so on [10]–[12]. Considering the above advantages, ISAC has been applied in diverse scenarios, such as autonomous vehicle networks [13], smart home networks [14], and Internet of Things (IoT) [15].

Recently, security issues have attracted considerable attention due to the inherent openness of wireless channels, which makes them highly susceptible to eavesdropping [16]. To overcome this challenge, information encryption and physical layer security have been widely adopted in wireless networks to protect the transmitted information from being decrypted [17]. However, with the increasing security requirements, the transmission behavior should be hidden in some specific scenarios [18]. As a result, covert communication emerges to provide a higher level of security [19]. Bash *et al*. first investigated the fundamental performance limit of covert communications. They proposed the square root law that the transmitter can only transmit at most $\mathcal{O}\left(\sqrt{n}\right)$ bits of information in n channel uses over the additive white Gaussian noise channel, and $\lim_{n\to\infty} \mathcal{O}\left(\sqrt{n}\right)/n = 0$, indicating the zero covert rate [20]. In addition, the performance of covert communications can be severely degraded due to the inevitable multi-path fading and interference [21]. To overcome these limitations, noise and channel uncertainty are further exploited to create additional confusion for warden's detection [22], and various advanced technologies are used to increase the covert transmission rate, such as IRS [23] and artificial noise [24].

Specifically, a significant number of papers have devoted to proposing covert schemes against multiple wardens, which is much more common in real-world scenarios [25]–[29]. In [25], Soltani *et al*. firstly demonstrated that Alice can covertly transmit $\mathcal{O}\left(\min\left\{n, m^{\frac{\gamma}{2}}\sqrt{n}\right\}\right)$ bits of information to Bob on n channel uses with m wardens, where γ denotes the path-

Manuscript received October 7, 2024; revised January 15, 2025 and April 10, 2025; accepted May 23, 2025. The work of N. Zhao was supported in part by the National Natural Science Foundation of China (NSFC) under Grant U23A20271, 62325103 and 62271099. An earlier version of this paper was presented in part at IEEE ICC 2025 [1]. The associate editor coordinating the review of this paper and approving it for publication was B. Makki. *(Corresponding author: Nan Zhao.)*

Y. Wu and N. Zhao are with the School of Information and Communication Engineering, Dalian University of Technology, Dalian 116024, China. (e-mail: wuyj@mail.dlut.edu.cn, zhaonan@dlut.edu.cn)

C. Xing is with the School of Information and Electronics, Beijing Institute of Technology, Beijing 100081, P. R. China. (e-mail: xingchengwen@gmail.com)

J. Tang is with the School of Electronic and Information Engineering, South China University of Technology, Guangzhou 510641, China. (e-mail: eejtang@scut.edu.cn)

X. Y. Zhang is with the Engineering Research Center of Short-Distance Wireless Communications and Network, Ministry of Education, School of Microelectronics, South China University of Technology, Guangzhou 510641, China. He is also with Pazhou Lab. (e-mail: zhangxiuyin@scut.edu.cn)

K. K. Wong is with the Department of Electronic and Electrical Engineering, University College London, Torrington Place, WC1E 7JE, United Kingdom and he is also with Yonsei Frontier Lab, Yonsei University, Seoul, Korea. (email: kai-kit.wong@ucl.ac.uk)

George K. Karagiannidis is with Department of Electrical Engineering, Taif University, Taif, Saudi Arabia, and also with the Department of Electrical and Computer Engineering, Aristotle University of Thessaloniki, 54124 Thessaloniki, Greece. (e-mail: geokarag@auth.gr)

loss. Forouzesh *et al*. jointly considered covert communication and secure transmission for an untrusted relaying network with multiple wardens in [26]. Jiang *et al*. investigated the covert communication schemes in D2D underlaying cellular networks against a single or multiple wardens in [27]. Arghavani *et al*. tackled the problem of finite blocklength covert communication in the presence of multiple colluding wardens adopting maximal ratio combining based detection strategy, and proposed a zero-sum game formulation to model the interaction among the transmitter, the jammer, and wardens in [28]. Considering the high mobility of UAV, Mao *et al*. studied UAV-aided ground-to-air covert network in [29], and jointly optimized user association, bandwidth allocation, transmit power control and UAV 3-D deployment to maximize the transmission rate with multiple wardens.

While ISAC is inevitably threatened by eavesdropping risks due to the inherent openness, the higher level security of covert communication makes its application in ISAC effective in improving ISAC security [30]. How to design a covert ISAC has sparked a hot discussion since it is of great significance in maintaining national security, promoting the development of healthy IoT, and satisfying users' privacy requirements [31]. At present, research on covert ISAC is in its infancy, and there are only a few initial works [31]–[35]. Ma *et al*. proposed a basic covert beamforming framework to maximize mutual information (MI) and covert rate in [31], where MI is used to measure the sensing performance. In [32], Hu *et al*. maximized the covert throughput while ensuring a high probability of radar sensing, thus achieving the trade-off between radar sensing and covert transmission. Zhang *et al*. formulated an alternative optimization method for the IRS-aided covert ISAC to maximize the covert rate in [33]. In addition, Chen *et al*. proposed an active IRS-assisted covert NOMA-ISAC scheme and maximized the covert rate by jointly optimizing the transmission and reflection beamformings [34]. However, the above works only focus on the case of a single warden, and the covert ISAC against multiple wardens receives less attention. Ghosh *et al.* proposed a covert ISAC scheme with multiple wardens in [35], but the wardens can not cooperative with each other.

Motivated by the above, we focus on the covert ISAC against collusive wardens in this paper. The main contributions and motivations are summarized as follows.

- To the best of our knowledge, there remains a research gap in investigating covert ISAC under cooperative detection scenarios. To address this, we propose a novel covert ISAC network where the transmitter Alice simultaneously communicates with the legitimate user Bob and senses an aerial target while evading collusive wardens, which is more practical, complex and challenging compared to the existing work considering a single warden.
- We develop a quantitative model to characterize the detection performance of collusive wardens. The analysis demonstrates that while collusive detection can significantly improve performance, the sensing signal degrades performance as interference. Moreover, we derive the optimal detection threshold for each warden to minimize GDOP, creating the worst situation for covert ISAC. Notably, the covert ISAC network designed under the extreme condition exhibits enhanced robustness.
- We aim to maximize the covert transmission rate via jointly optimizing the transmission and sensing beamformings, where the covertness constraint, sensing constraint and transmit power constraint are considered. To tackle this non-convex problem, the unitary-iteration (UI) beamforming and zero-forcing (ZF) beamforming are respectively proposed to transform it into convex ones by applying the successive convex approximation (SCA) and semidefinite relaxation.
- Numerical results demonstrate the fundamental trade-off among communication, sensing and covertness, offering insights for practical system design. The comparison with three benchmark schemes confirm the effectiveness of our proposed ZF and UI schemes in practical covert ISAC scenarios. Furthermore, the results conclusively demonstrate that optimized beamforming design combined with power allocation can significantly enhance covert communication performance.

The rest of this paper is organized as follows. In Section II, the system model is portrayed. In Section III, the wardens' detection performance is analyzed, and the optimal detection threshold of each warden is derived. In Section IV, the optimization problem is formulated and two schemes are proposed to solve it. Simulation results are illustrated in Section V with the conclusion in Section VI.

Notation: Scalars and vectors are denoted by italic letters and bold-face letters, respectively. $\mathbb{C}$ is the complex number set. $|\cdot|$ denotes the absolute value of complex scalar. $(\cdot)^T$ and $(\cdot)^H$ represent the transpose and the conjugate transpose of a matrix, respectively. $\Pi(\cdot)$ denotes the continuous multiplication. $\Pr(A)$ is the probability of the occurrence of an event A. $\mathbb{E}(x)$, $f(x)$ and $\mathcal{F}(x)$ are the expectation, the probability density function (PDF) and the cumulative distribution function (CDF) of a random variable x, respectively. $||\mathbf{x}||_2$ represents the Euclidean norm of $\mathbf{x}$. $\mathbf{I}_N$ represents the $N \times N$ identity matrix. $\mathbb{C}^{N\times N}$ is the set of $N \times N$ complex matrices. $x \sim \mathcal{CN}(\mu, \sigma^2)$ denotes the circularly symmetric complex Gaussian distribution with the mean μ and variance σ^2. $\mathrm{Tr}(\mathbf{S})$ and $\mathrm{Ra}(\mathbf{S})$ respectively denote the trace and rank of the square matrix $\mathbf{S}$.

II. System Model

A. Network Model

As shown in Fig. 1, we consider a covert ISAC network against randomly distributed Willies. To be specific, an uniform linear array transmitter Alice with M antennas along x-axis communicates with a single-antenna receiver Bob while keeping sensing an aerial target. Considering a practical internet-of-things scenario, we investigate a clustering-based detection, where multiple single-antenna Willies collaborate with each other to monitor the legitimate communication. In addition, we employ a three-dimensional cylindrical coordinate system, where Alice, Bob and the target are located at $\mathcal{A} = (0, 0, 0)$, $\mathcal{B} = (r_b, \varphi_b, 0)$ and $\mathcal{G} = (r_t, \varphi_t, H)$, respectively. Assume that the T Willies are independently

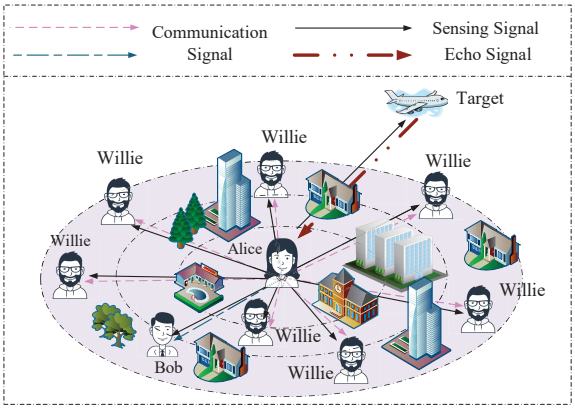

Fig. 1. Covert ISAC against randomly distributed Willies.

and uniformly distributed in a circular area with radius of D centered at Alice. The location of the t-th Willie is denoted as $\mathcal{W}_t(r_{wt}, \varphi_{wt}, 0), t \in \mathcal{T}, \mathcal{T} = \{1, 2, \ldots, T\}$, which follows a binomial point process (BPP), i.e., $\mathcal{W}_t \sim \Phi_w$. [1]

B. Communication Channel Model

The channel from Alice to Bob follows the large-scale path loss and Rayleigh fading [36], and the complex channel gain can be given as

$$\mathbf{g}_{ab} = \sqrt{\rho_0 r_{ab}^{-\alpha_g}} \mathbf{h}_{ab} \in \mathbb{C}^{M\times 1}, \tag{1}$$

where $\mathbf{h}_{ab}$ is modeled as complex Gaussian distributed, i.e., $\mathbf{h}_{ab} \sim \mathcal{CN}(\mathbf{0}, \mathbf{I}_M)$, ρ_0 denotes the power gain at the reference distance of 1 m, α_g is the terrestrial path-loss exponent, and r_{ab} is the distance between Alice and Bob.

Similarly, the channel between Alice and the t-th Willie is also determined by both the large-scale path loss and small-scale Rayleigh fading, which can be modeled as

$$\mathbf{g}_{aw_t} = \sqrt{\rho_0 r_{aw_t}^{-\alpha_g}} \mathbf{h}_{aw_t} \in \mathbb{C}^{M\times 1}, t \in \mathcal{T}, \tag{2}$$

where $\mathbf{h}_{aw_t} \sim \mathcal{CN}(\mathbf{0}, \mathbf{I}_M)$, and r_{aw_t} denotes the distance between Alice and the t-th Willie.

To sense the target, Alice consistently generates sensing signal and receives the echo. Furthermore, to enhance the covertness of the transmission, the communication signal is transmitted with a prior transmission probability in each time slot. To confuse Willies, Alice decides whether to transmit or not with equal probabilities, i.e., $p_1 = p_0 = 0.5$ [19].

Assume that $x_s[i]$ is the deterministic sensing signal of the i-th channel use with $\mathbb{E}\left(|x_s[i]|^2\right) = 1$, and $\mathbf{u}_s \in \mathbb{C}^{M\times 1}$ denotes the precoding vector for sensing, $i \in \mathcal{L}, \mathcal{L} = \{1, 2, \ldots, L\}$, and L is the number of available channel uses. Thus, when only the sensing signal is transmitted, the received signal at Bob can be expressed as

$$\mathrm{y}_{\mathrm{B}}[i] = \mathbf{g}_{ab}^H \mathbf{u}_s x_s[i] + n_{\mathrm{B}}[i], i \in \mathcal{L}, \tag{3}$$

[1]The model can be well extended to the case of multiple legitimate multi-antenna users, which will be investigated in our future work.

and the received signal at the t-th Willie can be expressed as

$$\mathrm{y}_{\mathrm{W}_t}[i] = \mathbf{g}_{aw_t}^H \mathbf{u}_s x_s[i] + n_{\mathrm{W}_t}[i], i \in \mathcal{L}, \tag{4}$$

where $n_{\mathrm{B}}[i] \sim \mathcal{CN}\left(0, \sigma_b^2\right)$ and $n_{\mathrm{W}_t}[i] \sim \mathcal{CN}\left(0, \sigma_{w_t}^2\right)$ denote the additive white Gaussian noise (AWGN) at Bob and the t-th Willie, respectively.

When the communication and sensing signals are simultaneously transmitted, the received signal in the i-th channel use at Bob can be described as

$$\mathrm{y}_{\mathrm{B}}[i] = \mathbf{g}_{ab}^H \mathbf{u}_s x_s[i] + \mathbf{g}_{ab}^H \mathbf{u}_c x_c[i] + n_{\mathrm{B}}[i], i \in \mathcal{L}, \tag{5}$$

and the corresponding received signal at the t-th Willie can be represented as

$$\mathrm{y}_{\mathrm{W}_t}[i] = \mathbf{g}_{aw_t}^H \mathbf{u}_s x_s[i] + \mathbf{g}_{aw_t}^H \mathbf{u}_c x_c[i] + n_{\mathrm{W}_t}[i], i \in \mathcal{L}, \tag{6}$$

where $x_c[i]$ is the transmitted communication signal with $\mathbb{E}\left(|x_c[i]|^2\right) = 1$, and Alice precodes the communication signal with the vector $\mathbf{u}_c \in \mathbb{C}^{M\times 1}$.

Accordingly, the signal-to-interference-plus-noise ratio (SINR) at Bob can be expressed as

$$\gamma_b = \frac{|\mathbf{g}_{ab}^H \mathbf{u}_c|^2}{|\mathbf{g}_{ab}^H \mathbf{u}_s|^2 + \sigma_b^2}, \tag{7}$$

and the transmission rate between Alice and Bob can be represented as

$$R = \log_2(1 + \gamma_b) = \log_2\left(1 + \frac{|\mathbf{g}_{ab}^H \mathbf{u}_c|^2}{|\mathbf{g}_{ab}^H \mathbf{u}_s|^2 + \sigma_b^2}\right). \tag{8}$$

Without loss of generality, we consider to adopt the transmission rate in (8) subject to the covertness constraint as a measure of communication quality, which is also known as the covert transmission rate (CTR) [37].

C. Sensing Channel Model

Consider that the channel between Alice and aerial target is line-of-sight. In addition, due to the terrestrial environment, the echoes reflected from Bob and Willies can be negligible.

Accordingly, the echo signal at Alice with only sensing performed can be expressed as

$$\mathrm{y}_{\mathrm{A}}[i] = \mu \mathbf{a}_T \mathbf{a}_R^H \mathbf{u}_s x_s[i] + \mathbf{n}_{\mathrm{A}}[i] = \Xi \mathbf{u}_s x[i] + \mathbf{n}_{\mathrm{A}}[i], \tag{9}$$

where $\Xi = \mu \mathbf{a}_T \mathbf{a}_R^H$, and μ is the complex amplitude related to the round-trip path-loss and the reflection factor of target. Moreover, $\mathbf{a}_T$ and $\mathbf{a}_R$ respectively denote the transmit steering vector and receive steering vector, which can be expressed as

$$\mathbf{a}_T = \mathbf{a}_R = \left[1, e^{\frac{-j2\pi d\psi}{\lambda}}, \ldots, e^{\frac{-j2\pi d(M-1)\psi}{\lambda}}\right]^T \in \mathbb{C}^{M\times 1}, \tag{10}$$

where $\psi = \sin\theta \cos\varphi_t$ with $\theta = \arccos\frac{H}{r_t}$. Note that d denotes the spacing between the adjacent antennas, and λ denotes the carrier wavelength. In addition, $\mathbf{n}_A[i] \sim \mathcal{CN}(\mathbf{0}, \sigma_a^2 \mathbf{I}_M)$ denotes the AWGN at Alice.

The echoes can offer additional details of the target and channel state information (CSI), enabling the transmitter to gain a more comprehensive understanding and diminish *a priori* uncertainty regarding the target. Accordingly, MI can serve as a measure to assess the quantity of information acquired by the transmitter from the echoes.

Given $\mathrm{y_A}[i]$ in (9), the MI with no communication signal can be expressed as

$$I_1 = \frac{1}{2}\log_2\left(1+\frac{\mathbf{u}_s^H\Xi^H\Xi\mathbf{u}_s}{\sigma_a^2}\right). \tag{11}$$

For the other case, the corresponding echo signal at Alice can be expressed as

$$\mathrm{y_A}[i] = \Xi\mathbf{u}_s x_s[i] + \Xi\mathbf{u}_c x_c[i] + \mathbf{n_A}[i], \tag{12}$$

with its MI given by

$$I_2 = \frac{1}{2}\log_2\left(1+\frac{\mathbf{u}_s^H\Xi^H\Xi\mathbf{u}_s}{\mathbf{u}_c^H\Xi^H\Xi\mathbf{u}_c+\sigma_a^2}\right). \tag{13}$$

Remark 1: It has been demonstrated that increasing MI results in greater information acquisition of the transmitter, consequently enhancing the recognition capability [31]. To ensure the performance of sensing, we should guarantee that the MI is above a preset threshold.

III. Detection Analysis and Optimization

In this section, we analyze each Willie's detection outage probability (DOP), and derive their optimal thresholds to enhance the collaborative detection performance.

A. Detection Analysis

Assume that Willies possess full knowledge of CSI, as well as the prior transmission probability and transmission power, which enables them to design the optimal detectors to achieve the optimal detection, creating the worst case for Alice [37].

According to [18], Willies can analyze the received power with a radiometer to determine whether Alice is transmitting. Therefore, the t-th Willie is required to address a binary hypothesis testing as

$$\mathrm{y_{W_t}}[i]=\begin{cases}\mathbf{g}_{aw_t}^H\mathbf{u}_s x_s[i]+n_{\mathrm{W}_t}[i], t\in\mathcal{T}, & \mathcal{H}_0,\\ \mathbf{g}_{aw_t}^H\mathbf{u}_s x_s[i]+\mathbf{g}_{aw_t}^H\mathbf{u}_c x_c[i]+n_{\mathrm{W}_t}[i], & \mathcal{H}_1,\end{cases} \tag{14}$$

where $\mathcal{H}_0$ is the null hypothesis suggesting that Alice does not engage in transmitting, while $\mathcal{H}_1$ is the alternative hypothesis proposing that Alice performs transmitting.

Actually, the optimal test for each Willie is proven to be the threshold test [38]. Based on the average received power, the decision rule of the t-th Willie can be described as

$$\overline{P}_{w_t} \underset{\mathcal{D}_0}{\overset{\mathcal{D}_1}{\gtrless}} \overline{\xi}_t, \tag{15}$$

where

$$\overline{P}_{w_t} = \frac{1}{L}\sum_{i=1}^{L}\left|\mathrm{y_{W_t}}[i]\right|^2, \tag{16}$$

and $\overline{\xi}_t > 0$ is the t-th Willie's detection threshold. Note that $\mathcal{D}_1$ is the binary decision demonstrating that the transmission occurs with $\overline{P}_{w_t} > \overline{\xi}_t$. On the contrary, $\mathcal{D}_0$ indicates that Alice keeps silent with $\overline{P}_{w_t} < \overline{\xi}_t$.

According to [39], the number of the available channel uses in each time slot is proportional to the bandwidth. Thus, we can conclude that the available channel uses can be increased to approach infinity with sufficient communication bandwidth. Therefore, $L \to \infty$ is considered in each time slot, and the average received power at the t-th Willie can be approximated as a stationary statistical random variable expressed as

$$P_{w_t} = \lim_{L\to\infty}\overline{P}_{w_t} = \begin{cases} S_{w_{tc}} + S_{w_{ts}} + \sigma_{w_t}^2, & \mathcal{H}_1,\\ S_{w_{ts}} + \sigma_{w_t}^2, & \mathcal{H}_0,\end{cases} \tag{17}$$

where

$$S_{w_{tc}} = \frac{\rho_0|\mathbf{h}_{aw_t}^H\mathbf{u}_c|^2}{r_{aw_t}^{\alpha_g}} \tag{18}$$

and

$$S_{w_{ts}} = \frac{\rho_0|\mathbf{h}_{aw_t}^H\mathbf{u}_s|^2}{r_{aw_t}^{\alpha_g}} \tag{19}$$

are the average statistical powers of the sensing and communication, respectively.

Due to the uncertainty introduced by random variables, Willies will inevitably make two kinds of errors during the detection, including the miss detection (MD) and false alarm (FA). To be specific, MD happens when Alice actually performs transmitting while the t-th Willie fails to detect, i.e.,

$$S_{w_{tc}} + S_{w_{ts}} + \sigma_{w_t}^2 < \overline{\xi}_t. \tag{20}$$

By contrast, FA occurs when the t-th Willie determines that the transmission exists while Alice remains silent it, i.e.,

$$S_{w_{ts}} + \sigma_{w_t}^2 > \overline{\xi}_t. \tag{21}$$

Based on the decision rule in (15), the probability of the t-th Willie making a wrong detection can be given as

$$p_{w_t} = \Pr\{\mathcal{H}_1\}\Pr\{\mathcal{D}_0|\mathcal{H}_1\} + \Pr\{\mathcal{H}_0\}\Pr\{\mathcal{D}_1|\mathcal{H}_0\}, \tag{22}$$

where

$$\Pr\{\mathcal{H}_1\} = p_1 = 0.5,\ \Pr\{\mathcal{H}_0\} = p_0 = 0.5. \tag{23}$$

According to

$$\Pr\{\mathcal{D}_0|\mathcal{H}_1\} = \Pr\{S_{w_{tc}} + S_{w_{ts}} + \sigma_{w_t}^2 < \overline{\xi}_t\} \tag{24}$$

and

$$\Pr\{\mathcal{D}_1|\mathcal{H}_0\} = \Pr\{S_{w_{ts}} + \sigma_{w_t}^2 > \overline{\xi}_t\}, \tag{25}$$

p_{w_t} can be further formulated as

$$p_{w_t} = \begin{cases} 0, & S_{w_{ts}} < \xi_t < S_{w_{tc}} + S_{w_{ts}},\\ 0.5, & otherwise,\end{cases} \tag{26}$$

where $\xi_t = \overline{\xi}_t - \sigma_{w_t}^2$.

Without loss of generality, we define the probability that each Willie makes the error decision as DOP, and the t-th Willie's DOP can be formulated as

$$p_{d_t} = 1 - \Pr\{p_{w_t} = 0\} = 1 - \Pr\{S_{w_{ts}} < \xi_t < S_{w_{tc}} + S_{w_{ts}}\}, \tag{27}$$

and $0 \le p_{d_t} \le 1$. Specifically, $p_{d_t} = 0$ signifies that the t-th Willie can accurately perform detecting, and $p_{d_t} = 1$ indicates that he only makes a blind guess. The specific closed-form expression of p_{d_t} is provided in Proposition 1.

Proposition 1: The closed-form expression of p_{d_t} can be expressed as

$$P_{d_t} = \begin{cases} 1 - \dfrac{a_{ts}\left(e^{-a_{ts}\xi_t} - e^{-a_{tc}\xi_t}\right)}{a_{tc} - a_{ts}}, & a_{tc} \neq a_{ts}, \\ 1 - a_{tc}\xi_t e^{-a_{tc}\xi_t}, & a_{tc} = a_{ts}, \end{cases} \tag{28}$$

with

$$a_{ts} = \frac{r_{aw_t}^{\alpha_g}}{\rho_0 P_{as}}, \tag{29}$$

and

$$a_{tc} = \frac{r_{aw_t}^{\alpha_g}}{\rho_0 P_{ac}}, \tag{30}$$

where $P_{as} \triangleq \|\mathbf{u}_s\|_2^2$ and $P_{ac} \triangleq \|\mathbf{u}_c\|_2^2$ denote the powers of sensing and communication, respectively.

Proof: Please refer to Appendix A. ∎

B. Detection Optimization of Willies

Willies collaborate on detecting the legitimate transmission with the covert transmission outage taking place when at least one Willie successfully detects it. With this context, the global DOP (GDOP) is defined to quantify the likelihood of all Willies failing to detect the transmission as

$$p_e = \mathbb{E}_{\Phi_w}\left[\Pr\left\{\bigcap_{w_t \in \Phi_w} p_{w_t} \neq 0\right\}\right] = \mathbb{E}_{\Phi_w}\left[\prod_{w_t \in \Phi_w} p_{d_t}\right]. \tag{31}$$

Based on (28), the closed-form expression of GDOP is presented in Proposition 2.

Proposition 2: Considering the DOP of each Willie, the GDOP can be calculated as

$$p_e = \left[\int_0^D p_{d_t} \frac{2r}{D^2} dr\right]^T, \tag{32}$$

where p_{d_t} is given in (28) with $r_{aw_t} = r, t \in \mathcal{T}$.

Proof: As mentioned in Section II, Willies are independent and identically distributed and follow a BPP distribution within a circular area. Consequently, the probability density function (PDF) can be expressed as

$$f_{w_t}(r, \theta) = \frac{r}{\pi D^2}, \tag{33}$$

and (31) can be rewritten as

$$p_e = \prod_{t=1}^{T} \int_0^{2\pi} \int_0^D p_{d_t} \frac{r}{\pi D^2} dr d\theta = \prod_{t=1}^{T} \int_0^D p_{d_t} \frac{2r}{D^2} dr, \tag{34}$$

which can be further derived to be (32). ∎

According to (28), it is evident that the detection threshold significantly impacts the DOP. Thus, each Willie aims to identify its own optimal detection threshold to reduce the DOP and consequently minimize the GDOP. The optimal detection threshold of each Willie is detailed in Proposition 3.

Proposition 3: The optimal detection threshold of the t-th Willie is derived as

$$\xi_t^* = \begin{cases} \dfrac{\ln a_{ts} - \ln a_{tc}}{a_{ts} - a_{tc}}, & a_{tc} \neq a_{ts}, \\ \dfrac{1}{a_{tc}}, & a_{tc} = a_{ts}. \end{cases} \tag{35}$$

Proof: Please refer to Appendix B. ∎

Adopting the optimal detection threshold in (35), the minimum DOP achieved by the t-th Willie $p_{d_t}^\dagger$ can be calculated. When $a_{tc} \neq a_{ts}$, $p_{d_t}^\dagger$ can be expressed as

$$\begin{aligned} p_{d_t}^\dagger &= 1 - \frac{a_{ts}}{a_{tc} - a_{ts}} \left(e^{-\frac{a_{ts} \ln \frac{a_{ts}}{a_{tc}}}{a_{ts} - a_{tc}}} - e^{-\frac{a_{tc} \ln \frac{a_{ts}}{a_{tc}}}{a_{ts} - a_{tc}}}\right) \\ &= 1 - \frac{a_{ts}}{a_{tc} - a_{ts}} \left[\left(\frac{a_{ts}}{a_{tc}}\right)^{\frac{a_{ts}}{a_{tc} - a_{ts}}} - \left(\frac{a_{ts}}{a_{tc}}\right)^{\frac{a_{tc}}{a_{tc} - a_{ts}}}\right] \\ &\xrightarrow{r = \frac{a_{ts}}{a_{tc} - a_{ts}}} 1 - r\left[\left(\frac{a_{ts}}{a_{tc}}\right)^r - \left(\frac{a_{ts}}{a_{tc}}\right)^{r+1}\right] \\ &= 1 - r\left(1 - \frac{a_{ts}}{a_{tc}}\right)\left(\frac{a_{ts}}{a_{tc}}\right)^r = 1 - \left(\frac{a_{tc}}{a_{ts}}\right)^{\frac{a_{tc}}{a_{ts} - a_{tc}}}, \end{aligned} \tag{36}$$

and when $a_{tc} = a_{ts}$, $p_{d_t}^\dagger$ is equal to

$$p_{d_t}^\dagger = 1 - e^{-1}. \tag{37}$$

Hence, the minimum DOP of the t-th Willie can be derived as

$$p_{d_t}^\dagger = \begin{cases} 1 - \left(\dfrac{a_{tc}}{a_{ts}}\right)^{\frac{a_{tc}}{a_{ts} - a_{tc}}}, & a_{tc} \neq a_{ts}, \\ 1 - e^{-1}, & a_{tc} = a_{ts}. \end{cases} \tag{38}$$

Accordingly, the optimal GDOP can be calculated as

$$p_e^\dagger = \prod_{t=1}^{T} \int_0^{2\pi} \int_0^D p_{d_t}^\dagger \frac{r}{\pi D^2} dr d\theta = \left(p_{d_t}^\dagger\right)^T, \tag{39}$$

which can be further elaborated as

$$p_e^\dagger = \begin{cases} \left(1 - \left(\dfrac{P_{as}}{P_{ac}}\right)^{\frac{P_{as}}{P_{ac} - P_{as}}}\right)^T, & P_{ac} \neq P_{as}, \\ \left(1 - e^{-1}\right)^T, & P_{ac} = P_{as}. \end{cases} \tag{40}$$

When $p_e^\dagger$ exceeds a specified threshold, the collaborative detection fails. From (40), it can be noted that the optimal GDOP is not related to M, indicating that increasing or decreasing the number of antennas have no impact on Willies' collaborative detection.

Remark 2: Alice's transmit power is changing all the time. Thus, it is challenging for Willies to adjust the current thresholds to the optimal ones in time due to the delay. Nevertheless, we assume that all Willies still perform the detection with the optimal thresholds as the worst situation for the legitimate covert transmission.

We analyze the impacts of the number of Willies, and the sensing and communication powers on the GDOP, which are presented in Corollary 1 and Corollary 2, respectively.

Corollary 1: With the increasing number of Willies T, the optimal GDOP $p_e^\dagger$ decreases, however, this trend weakens when T is large enough.

Proof: Based on (40), $p_e^\dagger$ can be written as

$$p_e^\dagger = (1 - \varrho)^T, \tag{41}$$

where $\varrho = \left(\frac{P_{as}}{P_{ac}}\right)^{\frac{P_{as}}{P_{ac}-P_{as}}}$ or $\varrho = e^{-1}$. The first-order derivative of $p_e^\dagger$ with respect to T can be derived as

$$p_e^{\dagger'}(T) = (1-\varrho)^T \ln(1-\varrho), \tag{42}$$

and the second-order derivative of $p_e^\dagger$ with respect to T can be expressed as

$$p_e^{\dagger''}(T) = (1-\varrho)^T [\ln(1-\varrho)]^2. \tag{43}$$

Considering $0 < \varrho < 1$, we can conclude that $p_e^{\dagger'}(T) < 0$ and $p_e^{\dagger''}(T) > 0$. $p_e^{\dagger'}(T) < 0$ indicates that $p_e^\dagger$ monotonically decreases with T, and the detection performance can be upgraded by deploying more Willies. $p_e^{\dagger''}(T) > 0$ implies that the absolute value of $p_e^{\dagger'}(T)$ decreases as T increases, signifying a decrease in the slope of $p_e^\dagger$ with respect to T. This indicates that once a specific threshold is reached, the impact of increasing T on enhancing the detection performance becomes trivial. ■

Consequently, it is crucial to select an appropriate T to ensure the efficiency of surveillance.

Corollary 2: Increasing the sensing power P_{as} or decreasing communication power P_{ac} can both increase the optimal GDOP $p_e^\dagger$, provided that the two powers are unequal.

Proof: According to (41), it can be concluded that $p_e^\dagger$ monotonically decreases with respect to ϱ. The first-order derivative of ϱ with respect to P_{as} can be derived as

$$\varrho'(P_{as}) = \frac{\left(\frac{P_{as}}{P_{ac}}\right)^{P_{as}/(P_{ac}-P_{as})} H_{sc}}{(P_{ac}-P_{as})^2}, \tag{44}$$

and H_{sc} can be expressed as

$$H_{sc} = P_{ac} H_v, \tag{45}$$

where $H_v = \ln v - v + 1$ with $v = \frac{P_{as}}{P_{ac}}$. In addition, the first-order derivative of H_v with respect to v can be derived as

$$H_v'(v) = 1/v - 1, \tag{46}$$

which shows that $H_v'(v) > 0$ when $v < 1$ and $H_v'(v) < 0$ when $v > 1$, indicating that H_v first increases, and then decreases with v. Thus, H_v can achieve its maximum value at $v = 1$. Due to $H_v(1) = 0$, $H_v \le 0$ and $H_{sc} \le 0$ can be derived. According to (44), it is obvious that the positivity or negativity of $\varrho'(P_{as})$ depends on H_{sc}. Thus, $\varrho'(P_{as}) \le 0$ can be obtained, which states that ϱ monotonically decreases with respect to P_{as}. Furthermore, we can conclude that $p_e^\dagger$ monotonically increases with respect to P_{as}.

Similarly, the first-order derivative of ϱ with respect to P_{ac} can be derived as

$$\varrho'(P_{ac}) = \frac{-\left(\frac{P_{as}}{P_{ac}}\right)^{P_{ac}/(P_{ac}-P_{as})} H_{sc}}{(P_{ac}-P_{as})^2}, \tag{47}$$

and $\varrho'(P_{ac}) \ge 0$ can be accordingly obtained. Subsequently, we can conclude that $p_e^\dagger$ monotonically decreases with respect to P_{ac}. In summary, increasing P_{as} or decreasing P_{ac} can both increase $p_e^\dagger$, consequently reducing the detection performance. ■

IV. CTR Maximization

In this section, we jointly optimize the sensing vector $\mathbf{u}_s$ and transmission vector $\mathbf{u}_c$ to maximize the CTR while ensuring that MI remains above a preset threshold. Note that the optimization is achieved with all Willies adopting the optimal thresholds.

A. Problem Formulation

To maximize the CTR, the joint optimization problem can be formulated as

$$\begin{aligned}
\mathbf{P1}: \max_{\mathbf{u}_s,\mathbf{u}_c} \quad & R && \text{(48a)}\\
\text{s.t.} \quad & I_2 \ge \nu, && \text{(48b)}\\
& p_e^\dagger \ge 1-\varepsilon, && \text{(48c)}\\
& ||\mathbf{u}_c||_2^2 \le P_{\text{cmax}}, && \text{(48d)}\\
& ||\mathbf{u}_s||_2^2 \le P_{\text{smax}}. && \text{(48e)}
\end{aligned}$$

Note that (48b) serves as the MI constraint to guarantee the sensing performance, and $1-\varepsilon$ in (48c) is the minimum required GDOP with ε denoting the covertness level. P_{smax} and P_{cmax} represent the maximum available sensing and transmission powers, respectively.

Due to the highly coupled vectors, and non-convex objective function and constraints, it is difficult to solve $\mathbf{P1}$. To address this challenge, $\mathbf{P1}$ can be converted into a standard semi-definite programming (SDP).

First, the channels $\mathbf{g}_{ab}$ and $\mathbf{a}_T$ can be reformulated as

$$\mathbf{G}_{ab} = \mathbf{g}_{ab}\mathbf{g}_{ab}^H, \tag{49}$$

and

$$\mathbf{G}_T = \mathbf{a}_T\mathbf{a}_T^H. \tag{50}$$

Then, the Hermitian matrices of $\mathbf{u}_s$ and $\mathbf{u}_c$ can be obtained as

$$\mathbf{U}_c = \mathbf{u}_c\mathbf{u}_c^H \tag{51}$$

$$\mathbf{U}_s = \mathbf{u}_s\mathbf{u}_s^H, \tag{52}$$

which satisfy

$$\mathbf{U}_c \succeq 0, \text{Ra}(\mathbf{U}_c) = 1, \tag{53}$$

and

$$\mathbf{U}_s \succeq 0, \text{Ra}(\mathbf{U}_s) = 1. \tag{54}$$

Therefore, P_{ac} and P_{as} can be expressed as

$$P_{ac} = \text{Tr}(\mathbf{U}_c), P_{as} = \text{Tr}(\mathbf{U}_s). \tag{55}$$

According to the above transformation, $\mathbf{P1}$ can be recast as

$$\begin{aligned}
\mathbf{P2}: \max_{\mathbf{U}_s,\mathbf{U}_c} \quad & R && \text{(56a)}\\
\text{s.t.} \quad & (48b) \text{ and } (48c), && \text{(56b)}\\
& \text{Tr}(\mathbf{U}_c) \le P_{\text{cmax}}, && \text{(56c)}\\
& \text{Tr}(\mathbf{U}_s) \le P_{\text{smax}}, && \text{(56d)}\\
& \mathbf{U}_c \succeq 0, && \text{(56e)}\\
& \mathbf{U}_s \succeq 0, && \text{(56f)}\\
& \text{Ra}(\mathbf{U}_c) = \text{Ra}(\mathbf{U}_s) = 1. && \text{(56g)}
\end{aligned}$$

We propose two beamforming strategies to solve $\mathbf{P2}$ in the following subsections.

B. Unitary-Iteration Beamforming

In this subsection, we propose an unitary-iteration (UI) beamforming strategy. To begin with, we tackle the non-convex objective function along with associated constraints.

Due to the complex expression of CTR, we can rewrite R in (57) at the top, which is a concave-minus-concave expression. Thus, a global upper estimator of the concave expression $\widehat{R}(\mathbf{U}_s)$ can be afforded via the first-order Taylor expansion, which can be described with a given local point as

$$\begin{aligned}\widehat{R}(\mathbf{U}_s) \leq & \widehat{R}^{[lp]}(\mathbf{U}_s) = \widehat{R}\left(\mathbf{U}_s^{(p)}\right) + \\ & \mathrm{Tr}\left(\bigtriangledown^H_{\mathbf{U}_s^{(p)}} \widehat{R}\left(\mathbf{U}_s^{(p)}\right)\left(\mathbf{U}_s - \mathbf{U}_s^{(p)}\right)\right),\end{aligned} \tag{58}$$

where p denotes the iteration index, and $\mathbf{U}_s^{(p)}$ represent the optimized $\mathbf{U}_s$ in the p-th iteration. Note that $\widehat{R}(\mathbf{U}_s^{(p)})$ can be calculated by substituting $\mathbf{U}_s^{(p)}$ into (57) as

$$\widehat{R}\left(\mathbf{U}_s^{(p)}\right) = \log_2\left(\mathrm{Tr}\left(\mathbf{G}_{ab}\mathbf{U}_s^{(p)}\right) + \sigma_b^2\right). \tag{59}$$

In addition, $\bigtriangledown^H_{\mathbf{U}_s^{(p)}} \widehat{R}\left(\mathbf{U}_s^{(p)}\right)$ can be given by

$$\bigtriangledown^H_{\mathbf{U}_s^{(p)}} \widehat{R}\left(\mathbf{U}_s^{(p)}\right) = -\frac{1}{\ln 2}\frac{\mathbf{G}_{ab}}{\mathrm{Tr}\left(\mathbf{G}_{ab}\mathbf{U}_s^{(p)}\right) + \sigma_b^2}. \tag{60}$$

Thus, (56a) can be transformed into

$$\max_{\mathbf{U}_s, \mathbf{U}_c} \quad \widetilde{R} - \widehat{R}^{[lp]}(\mathbf{U}_s). \tag{61}$$

Moreover, Proposition 4 is proposed to convert (48b) into a convex constraint.

Proposition 4: (48b) can be converted as

$$\begin{aligned}&|\mu|^2\mathrm{Tr}\left(\mathbf{G}_T\mathbf{U}_s\right) \geq \\ &\quad (2^\nu - 1)\left(|\mu|^2\mathrm{Tr}\left(\mathbf{G}_T\mathbf{U}_c\right) + \frac{\sigma_a^2}{\mathrm{Tr}(\mathbf{G}_T)}\right).\end{aligned} \tag{62}$$

Proof: According to the channels in (50), (48b) can be recast as

$$\frac{1}{2}\log_2\left(1 + \frac{\mu|^2\mathrm{Tr}\left(\mathbf{G}_T\mathbf{U}_s\right)\mathrm{Tr}(\mathbf{G}_T)}{|\mu|^2\mathrm{Tr}\left(\mathbf{G}_T\mathbf{U}_c\right)\mathrm{Tr}(\mathbf{G}_T) + \sigma_a^2}\right) \geq \nu. \tag{63}$$

(63) can be further stated as

$$\frac{\mu|^2\mathrm{Tr}\left(\mathbf{G}_T\mathbf{U}_s\right)}{|\mu|^2\mathrm{Tr}\left(\mathbf{G}_T\mathbf{U}_c\right) + \frac{\sigma_a^2}{\mathrm{Tr}(\mathbf{G}_T)}} \geq 2^{2\nu} - 1, \tag{64}$$

which is equal to (62). ∎

In addition, because of the complex expression of the optimal GDOP $p_e^\dagger$, it is difficult to judge whether (48c) is convex. Thus, we rewrite it as

$$\left(1 - \left(\frac{P_{as}}{P_{ac}}\right)^{\frac{P_{as}}{P_{ac}-P_{as}}}\right)^T \geq 1 - \varepsilon. \tag{65}$$

Note that finding the square root of T of both sides of the inequality does not change inequality sign. Thus, we have

$$1 - \left(\frac{P_{as}}{P_{ac}}\right)^{\frac{P_{as}}{P_{ac}-P_{as}}} \geq \sqrt[T]{1-\varepsilon}, \tag{66}$$

which can be simplified as

$$\left(\frac{P_{as}}{P_{ac}}\right)^{\frac{P_{as}}{P_{ac}-P_{as}}} + \vartheta \leq 0, \tag{67}$$

where

$$\vartheta = \sqrt[T]{1-\varepsilon} - 1 < 0. \tag{68}$$

To handle the exponential function, the logarithmic function is introduced to transform (67) into

$$\frac{P_{as}}{P_{as}-P_{ac}}\ln\left(\frac{P_{as}}{P_{ac}}\right) + \ln\left(-\vartheta\right) \geq 0. \tag{69}$$

Unfortunately, it is still difficult to determine whether $\frac{P_{as}}{P_{as}-P_{ac}}\ln(\frac{P_{as}}{P_{ac}})$ is a convex or concave function. Therefore, we will solve the problem in two classifications, i.e., $P_{as} - P_{ac} > 0$ and $P_{as} - P_{ac} < 0$.

1) $P_{as} - P_{ac} > 0$:

With $P_{as} - P_{ac} > 0$, (69) can be transformed as

$$P_{as}\ln\left(\frac{P_{as}}{P_{ac}}\right) + \left(P_{as} - P_{ac}\right)\ln\left(-\vartheta\right) \geq 0, \tag{70}$$

For convenience, we define

$$f(P_{as}; P_{ac}) = P_{as}\ln\left(\frac{P_{as}}{P_{ac}}\right), \tag{71}$$

and the Hessian Matrix of $f(P_{as}; P_{ac})$ can be calculated as

$$\bigtriangledown^2 f(P_{as}; P_{ac}) = \begin{bmatrix} \frac{1}{P_{as}} & -\frac{1}{P_{ac}} \\ -\frac{1}{P_{ac}} & \frac{P_{as}}{P_{ac}^2} \end{bmatrix} \succeq 0. \tag{72}$$

According to (72), we can conclude that $\bigtriangledown^2 f(P_{as}; P_{ac})$ is a positive semi-definite matrix, indicating that $f(P_{as}; P_{ac})$ is convex. However, it is obvious that $(P_{as} - P_{ac})\ln(-\vartheta)$ is linear, and (70) is convex-plus-linear, which is not convex. Thus, we can similarly approximate $f(P_{as}; P_{ac})$ via the first-order Taylor expansion described as (74) at the top of the next page. In the same way, p denotes the iteration index, and

$$P_{as}^{(p)} = \mathrm{Tr}(\mathbf{U}_s^{(p)}), P_{ac}^{(p)} = \mathrm{Tr}(\mathbf{U}_c^{(p)}) \tag{73}$$

represent the optimized communication and sensing powers in the p-th iteration.

Based on the above conversion, (70) can eventually be transformed as

$$\widehat{f}(\mathrm{Tr}(\mathbf{U}_s); \mathrm{Tr}(\mathbf{U}_c)) + (\mathrm{Tr}(\mathbf{U}_s) - \mathrm{Tr}(\mathbf{U}_c))\ln\left(-\vartheta\right) \geq 0. \tag{75}$$

2) $P_{as} - P_{ac} \leq 0$:

Similarly, with $P_{as} - P_{ac} \leq 0$, (69) can also be converted as

$$f(P_{as}; P_{ac}) + \left(P_{as} - P_{ac}\right)\ln\left(-\vartheta\right) \leq 0, \tag{76}$$

which is a convex constraint, and can be re-written as

$$f(\mathrm{Tr}(\mathbf{U}_s); \mathrm{Tr}(\mathbf{U}_c)) + (\mathrm{Tr}(\mathbf{U}_s) - \mathrm{Tr}(\mathbf{U}_c))\ln\left(-\vartheta\right) \leq 0. \tag{77}$$

Henceforth, all the constraints are transformed into convex ones except for the rank-1 constraint, which can be relaxed to

$$R=\log_2\left(1+\frac{\mathrm{Tr}\left(\mathbf{G}_{ab}\mathbf{U}_c\right)}{\mathrm{Tr}\left(\mathbf{G}_{ab}\mathbf{U}_s\right)+\sigma_b^2}\right)=\log_2\left(\mathrm{Tr}\left(\mathbf{G}_{ab}\left(\mathbf{U}_c+\mathbf{U}_s\right)\right)+\sigma_b^2\right)-\log_2\left(\mathrm{Tr}\left(\mathbf{G}_{ab}\mathbf{U}_s\right)+\sigma_b^2\right)\triangleq\widetilde{R}-\widehat{R}\left(\mathbf{U}_s\right). \quad (57)$$

$$f(P_{as};P_{ac})\geq f(P_{as}^{(p)};P_{ac}^{(p)})+\left(\ln\frac{P_{as}^{(p)}}{P_{ac}^{(p)}}+1\right)(P_{as}-P_{as}^{(p)})-\frac{P_{as}^{(p)}}{P_{ac}^{(p)}}(P_{ac}-P_{ac}^{(p)})\triangleq\widehat{f}(P_{as};P_{ac}). \quad (74)$$

tackle the non-convex obstacle. Based on the above transformation, $\mathbf{P2}$ can be transformed into an SDP decomposed as

$$\begin{aligned}\mathbf{P3.1}:\max_{\mathbf{U}_s\succeq 0,\mathbf{U}_c\succeq 0}\quad & \widetilde{R}-\widehat{R}^{[lp]}(\mathbf{U}_s) && (78a)\\ \text{s.t.}\quad & (56c),(56d),(62),(75) && (78b)\\ & \mathrm{Tr}(\mathbf{U}_s-\mathbf{U}_c)>0, && (78c)\end{aligned}$$

and

$$\begin{aligned}\mathbf{P3.2}:\max_{\mathbf{U}_s\succeq 0,\mathbf{U}_c\succeq 0}\quad & \widetilde{R}-\widehat{R}^{[lp]}(\mathbf{U}_s) && (79a)\\ \text{s.t.}\quad & (56c),(56d),(62),(77) && (79b)\\ & \mathrm{Tr}(\mathbf{U}_s-\mathbf{U}_c)\leq 0, && (79c)\end{aligned}$$

which are both convex, and can be directly tackled via a standard convex optimization solver such as CVX.

With the identical channels, solving $\mathbf{P3.1}$ and $\mathbf{P3.2}$ can yield their own optimal solutions, and we can obtain the final solution to $\mathbf{P2}$ by comparing the optimal CTR achieved by the two sets of optimal solutions. The specific steps are detailed in Algorithm 1, where ς is the convergence estimation sign.

The computational complexity of Algorithm 1 mainly arises from solving (78) and (79), which both possess M^2+M^2 variables. Accordingly, the complexity of Algorithm 1 can be calculated as

$$\mathcal{O}\left(\mathcal{W}_1\left(2M^2\right)^{3.5}+\mathcal{W}_2\left(2M^2\right)^{3.5}\right), \quad (80)$$

where $\mathcal{W}_1$ and $\mathcal{W}_2$ refers to the numbers of iterations in solving $\mathbf{P3.1}$ and $\mathbf{P3.2}$, respectively [40], [41].

Algorithm 1 - UI beamforming for (56)

1: **Initialization**: Initialize $\mathbf{u}_s^{(0)}$, $\mathbf{u}_c^{(0)}$ and ς , and set the iteration index $l=0$, $a=0$. Calculate $R^{(0)}$ with the initial settings.
2: **repeat**
3: Update: $l=l+1$.
4: Optimize the beamforming vectors via (78).
5: **until** $R^{(l)}-R^{(l-1)}\leq\varsigma$.
6: **repeat**
7: Update: $a=a+1$.
8: Optimize the beamforming vectors via (79).
9: **until** $R^{(a)}-R^{(a-1)}\leq\varsigma$.
10: If $R^{(l)}>R^{(a)}$, $R^*=R^{(l)}$, $\mathbf{u}_s^*=\mathbf{u}_s^{(l)}$ and $\mathbf{u}_c^*=\mathbf{u}_c^{(l)}$.
11: If $R^{(l)}<R^{(a)}$, $R^*=R^{(a)}$, $\mathbf{u}_s^*=\mathbf{u}_s^{(a)}$ and $\mathbf{u}_c^*=\mathbf{u}_c^{(a)}$.
12: **Output**: $\mathbf{u}_s^*$, $\mathbf{u}_c^*$ and R^*.

C. Zero-Forcing Beamforming

Zero-forcing beamforming is highly recognized for its low complexity, ease of implementation and conversion. Therefore, we also adopt the zero-forcing beamforming, which is widely adopted in many works.

To eliminate the interferences at Bob and target, we design the zero-forcing (ZF) beamforming to satisfy

$$\mathbf{g}_{ab}^H\mathbf{u}_s=0, \quad (81)$$

and

$$\Xi\mathbf{u}_c=0, \quad (82)$$

which can be recast as

$$\mathrm{Tr}\left(\mathbf{G}_{ab}\mathbf{U}_s\right)=0, \quad (83)$$

and

$$\mathrm{Tr}\left(\mathbf{G}_T\mathbf{U}_c\right)=0. \quad (84)$$

Therefore, (48b) can be converted as

$$|\mu|^2\mathrm{Tr}\left(\mathbf{G}_T\mathbf{U}_s\right)\geq\left(2^{2\nu}-1\right)\frac{\sigma_a^2}{\mathrm{Tr}(\mathbf{G}_T)}. \quad (85)$$

Accordingly, $\mathbf{P2}$ can be rewritten as

$$\begin{aligned}\mathbf{P4}:\max_{\mathbf{U}_s,\mathbf{U}_c}\quad & \mathrm{Tr}\left(\mathbf{G}_{ab}\mathbf{U}_c\right) && (86a)\\ \text{s.t.}\quad & (48c),(56c),(56d),(56e),(56f),(56g),\\ & (83),(84),(85). && (86b)\end{aligned}$$

Similarly, the rank-1 constraint can be relaxed. With (48c), we can transform $\mathbf{P4}$ into two sub-problems as

$$\begin{aligned}\mathbf{P5.1}:\max_{\mathbf{U}_s\succeq 0,\mathbf{U}_c\succeq 0}\quad & \mathrm{Tr}\left(\mathbf{G}_{ab}\mathbf{U}_c\right) && (87a)\\ \text{s.t.}\quad & (56c),(56d),(75),(78c),(83),\\ & (84),(85), && (87b)\end{aligned}$$

and

$$\begin{aligned}\mathbf{P5.2}:\max_{\mathbf{U}_s\succeq 0,\mathbf{U}_c\succeq 0}\quad & \mathrm{Tr}\left(\mathbf{G}_{ab}\mathbf{U}_c\right) && (88a)\\ \text{s.t.}\quad & (56c),(56d),(77),(79c),(83),\\ & (84),(85), && (88b)\end{aligned}$$

which can both be directly solved via CVX. The optimal solution to $\mathbf{P4}$ can be obtained by comparing the optimal CTR achieved by $\mathbf{P5.1}$ and $\mathbf{P5.2}$. The specific steps of ZF-beamforming are characterized by Algorithm 2.

As no iteration is required to solve (88), the computational complexity arises mainly from solving (87), which also has

Algorithm 2 - ZF beamforming for (86)

1: **Initialization**: Initialize $\mathbf{u}_s^{(0)}$, $\mathbf{u}_c^{(0)}$ and ς , and set the iteration index $q = 0$. Calculate $R^{(0)}$ with the initial settings.
2: **repeat**
3: Update: $q = q + 1$.
4: Optimize the beamforming vectors via (87).
5: **until** $R^{(q)} - R^{(q-1)} \leq \varsigma$.
6: Optimize the beamforming vectors via (88), and record the optimization results as $R^{(h)}$, $\mathbf{u}_s^{(h)}$ and $\mathbf{u}_c^{(h)}$.
7: If $R^{(q)} > R^{(h)}$, $R^* = R^{(q)}$, $\mathbf{u}_s^* = \mathbf{u}_s^{(q)}$ and $\mathbf{u}_c^* = \mathbf{u}_c^{(q)}$.
8: If $R^{(q)} < R^{(h)}$, $R^* = R^{(h)}$, $\mathbf{u}_s^* = \mathbf{u}_s^{(h)}$ and $\mathbf{u}_c^* = \mathbf{u}_c^{(h)}$.
9: **Output**: $\mathbf{u}_s^*$, $\mathbf{u}_c^*$ and R^*.

$M^2 + M^2$ variables. Therefore, the complexity of Algorithm 2 can be calculated as

$$\mathcal{O}\left(\mathcal{V}_1 \left(2M^2\right)^{3.5}\right), \tag{89}$$

where $\mathcal{V}_1$ denotes the number of iterations in solving (87).

Remark 3: Due to the relaxation of the rank-1 constraint (56g), the rank of $\mathbf{U}_c^*$ and $\mathbf{U}_s^*$ may not be equivalent to 1. If

$$\mathrm{Ra}(\mathbf{U}_c^*) = \mathrm{Ra}(\mathbf{U}_s^*) = 1 \tag{90}$$

can be satisfied, the optimal vectors $\mathbf{u}_c^*$ and $\mathbf{u}_s^*$ can be decomposed via the singular value decomposition. Otherwise, the Gaussian randomization process can be adopted to attain the high-quality rank-1 solution.

Remark 4: As $\mathbf{P5.2}$ can be solved without iterations in the ZF beamforming strategy, we can get a conclusion that Algorithm 2 has lower complexity and faster rate compared to Algorithm 1.

V. Simulation Results

In this section, we evaluate the performance of the proposed covert ISAC scheme through simulation results. Unless explicitly specified, the relevant parameters are set according to the following defaults. Alice, Bob and the target are located at $\mathcal{A} = (0\mathrm{m}, 0, 0\mathrm{m})$, $\mathcal{B} = (50\mathrm{m}, \frac{\pi}{4}, 0\mathrm{m})$ and $\mathcal{G} = (60\mathrm{m}, \frac{3\pi}{4}, 150\mathrm{m})$, respectively. The radius is set as $D = 300$ m. The number of antennas equipped at Alice is $M = 8$, and the number of Willies is $T = 5$. Without loss of generality, the spacing between two adjacent antennas is assumed to be $d = 0.5\lambda$, and the azimuth angle is given as $\phi = \frac{\pi}{3}$. In addition, the air-to-ground and terrestrial path-loss exponents are set as $\alpha_s = 2$ and $\alpha_g = 2.8$, respectively. The path-loss gain at the reference distance is established as $\rho_0 = -40$ dB. Moreover, the noise power at Alice, Bob and the t-th Willie can be assumed as $\sigma_a^2 = \sigma_b^2 = \sigma_{w_t}^2 = -110$ dB. Finally, the covertness level is $\varepsilon = 0.1$.

The theoretical and simulated DOP p_{dt} and GDOP p_e with respect to the detection threshold ξ_t are presented in Fig. 2 with $P_{as} = 30$ mW and $P_{ac} = 10$ mW. In addition, the optimal GDOP is also displayed in Fig. 2 with Willies' optimal detection thresholds. First, we can observe that the theoretical and simulated values of DOP and GDOP can fit perfectly,

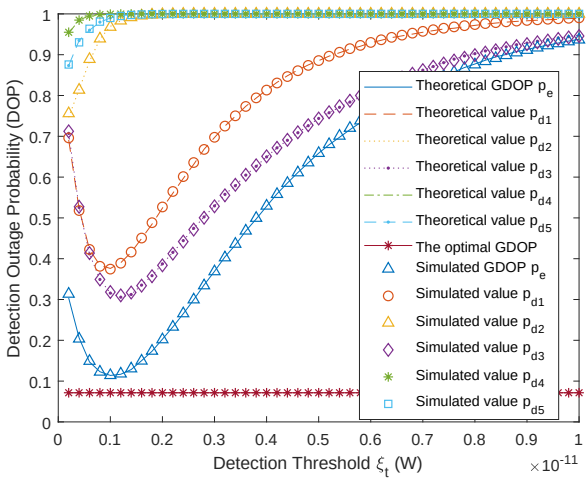

Fig. 2. Comparison of the DOP and GDOP under different detection threshold.

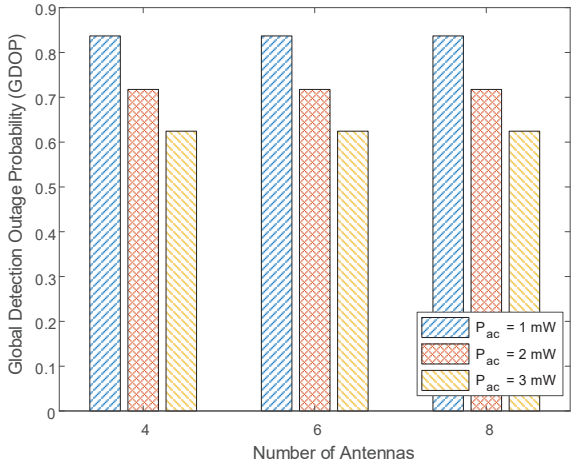

Fig. 3. Comparison of GDOP for different number of antennas M. $P_{ac} = 1$ mW, $P_{ac} = 2$ mW and $P_{ac} = 3$ mW are considered.

proving the derivation in Section III. Moreover, the DOP varies with ξ_t, and there exist different optimal detection thresholds for Willies to minimize the DOP. Furthermore, the GDOP is smaller than any DOP, indicating that Willies' cooperation is effective. We can conclude that the GDOP can be minimized when all Willies adopt their own optimal detection thresholds, which is in accordance with Proposition 3.

Fig. 3 illustrates the effects of the number of antennas M on the GDOP. Obviously, we can find that M cannot affect the GDOP no matter what value P_{ac} takes, which is consistent with the analysis in Section III. In other words, increasing or decreasing M will not impose an effect on Willies' detection performance. Thus, we can conclude that only the communication requirement need to be considered when designing M. In addition, the simulation results also show that the GDOP decreases as P_{ac} increases, which will be specifically discussed in Fig. 4.

Fig. 4 portrays the impacts of sensing and communication powers on GDOP with different number of Willies T. First, it can be observed that the GDOP decreases monotonically

This article has been accepted for publication in IEEE Transactions on Wireless Communications. This is the author's version which has not been fully edited and content may change prior to final publication. Citation information: DOI 10.1109/TWC.2025.3575033

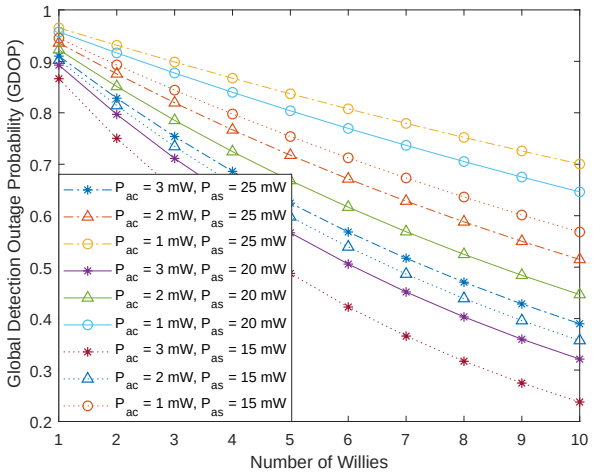

Fig. 4. Comparison of the influence of communication power P_{ac} and sensing power P_{as} on GDOP with different number of Willies T.

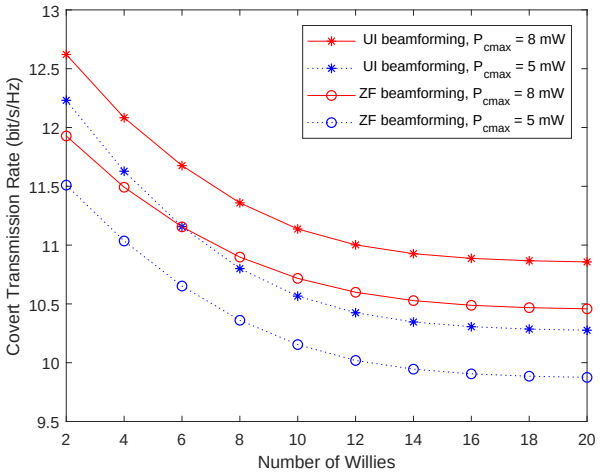

Fig. 6. Covert transmission rate achieved by UI and ZF beamformings versus the number of Willies T. $P_{\rm cmax} = 5$ mW and $P_{\rm cmax} = 8$ mW are considered.

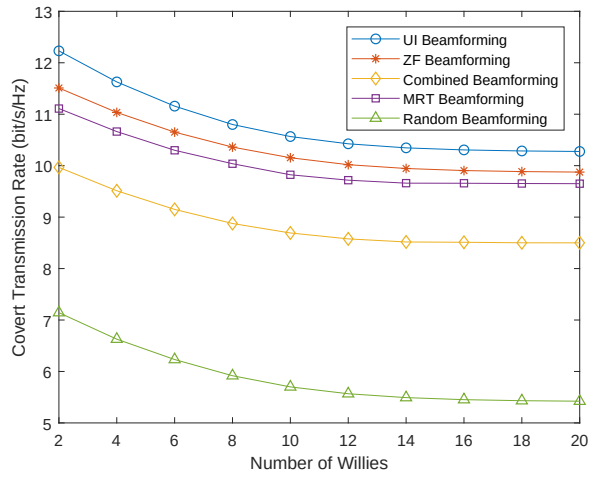

Fig. 5. Covert transmission rate versus the number of Willies T. Three benchmarks are considered.

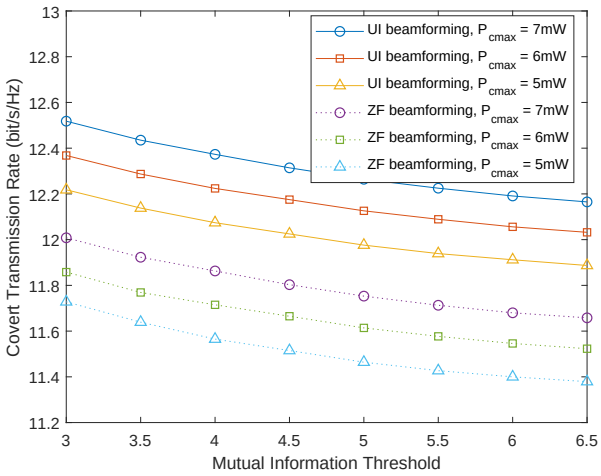

Fig. 7. Covert transmission rate achieved by UI and ZF beamformings versus different mutual information thresholds. $P_{\rm cmax} = 5$ mW, $P_{\rm cmax} = 6$ mW and $P_{\rm cmax} = 7$ mW are considered.

with increasing T, and a larger T leads to a much lower GDOP, which is consistent with Corollary 1. This observation also suggests that the choice of T should be based on a comprehensive consideration of both GDOP and detection efficiency. Furthermore, we observe that GDOP decreases as P_{ac} increases, which is due to the fact that higher P_{ac} results in greater received power at each Willie, thereby improving the correctness of its binary hypothesis testing. In contrast, the GDOP increases with P_{as}, due to the fact that the sensing signal acts as interference to Willies. Increasing P_{as} leads to more uncertainty for Willies, which consequently decreases detection performance of each Willie and eventually worsens the collusive detection performance.

We compare the two proposed schemes with three benchmarks in terms of CTR in Fig. 5 with $P_{\rm cmax} = 5$ mW and $P_{\rm smax} = 20$ mW. The "Combined Beamforming" benchmark represents the scenario where a beamforming is employed to simultaneously perform transmitting and sensing, i.e., $\mathbf{u}_s = \mathbf{u}_c$ [32]. The "MRT Beamforming" benchmark entails optimizing the communication beamforming $\mathbf{u}_c$ first via maximum ratio transmission (MRT), followed by optimizing the sensing beamforming $\mathbf{u}_s$ based on the optimized communication beamforming. The "Random Beamforming" benchmark means that the communication and sensing beamformings are randomly generated with the averaged CTR. From the results, it is evident that the CTRs achieved by the two proposed schemes (UI and ZF) are higher than those of benchmarks, demonstrating that optimizing the beamformings plays a crucial role in enhancing overall system performance. In addition, the CTR decreases as T increases. This is because increasing T contributes to wardens' detection performance, thereby posing a greater threat to covert transmission. Consequently, Alice is forced to reduce the communication power P_{ac} to ensure covertness, which results in a decrease in CTR, revealing the tarde-off between covertness and communication efficiency.

We illustrate the CTR achieved by the two proposed schemes as a function of the number of willies T in Fig. 6 with $P_{\rm cmax} = 5$ mW and $P_{\rm cmax} = 8$ mW. As expected, $P_{\rm cmax} = 8$ mW achieves a higher CTR. The improvement

This article has been accepted for publication in IEEE Transactions on Wireless Communications. This is the author's version which has not been fully edited and content may change prior to final publication. Citation information: DOI 10.1109/TWC.2025.3575033

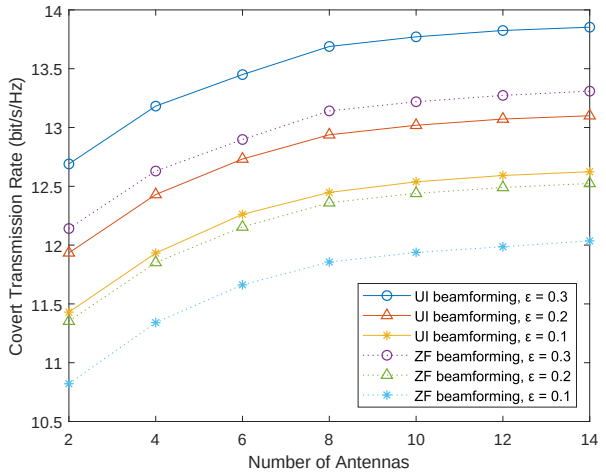

Fig. 8. Covert transmission rate achieved by UI and ZF beamformings versus the number of antennas. $\varepsilon = 0.1$, $\varepsilon = 0.2$ and $\varepsilon = 0.3$ are considered.

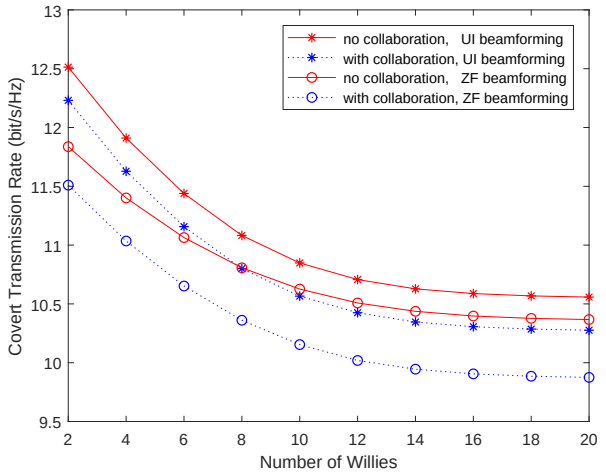

Fig. 9. Comparison of the covert transmission rate with and without cooperative eavesdropping.

stems from the fact that a higher P_{cmax} provides a wider and more flexible range for adjusting P_{ac} , thereby significantly enhancing the overall transmission efficiency. Furthermore, the results also demonstrate the superior performance of UI beamforming over ZF beamforming, which indicates that UI beamforming performs better in spite of its higher complexity, challenging the traditional cognition that complexity is directly proportional to performance.

We further investigate the influence of MI threshold on CTR in Fig. 7. As can be observed, the MI and CTR are a pair of metrics that constrain each other, which can not be both enhanced. The CTR decreases with the increasing MI threshold for both the two proposed schemes, which reveals the trade-off between sensing and communication. This decline can be attributed to that the communication signal is considered as interference during the sensing. Consequently, as the threshold becomes more stringent, Alice has to lower P_{ac} to satisfy the sensing requirement, resulting in a detrimental effect on the CTR. In addition, as shown in Fig. 7, the CTR increases with P_{cmax}, and the UI beamforming can achieve a higher CTR.

In Fig. 8, we study the impacts of the number of antennas M and covertness level ε on the CTR with $P_{\text{cmax}} = 5$ mW and $P_{\text{smax}} = 20$ mW. The results show that the covertness and CTR should be traded off, and the improvement of covertness can inevitably lead to the decrease of communication performance, and vice versa. First, it can be observed that the CTR increases with M, however, this trend tends to be slow. The results remind us that although increasing M does not pose an additional threat to the covert communication while increasing the transmission rate, it is essential to take into account the transmission efficiency in practical scenarios. Therefore, M should not to be too large. In addition, the CTR also increases with ε, because an increase in ε indicates that the requirement of covertness is relaxed. Thus, Alice can appropriately increase P_{ac} to improve the communication performance.

Fig. 9 compares the CTRs with and without collaborative eavesdropping with $P_{\text{cmax}} = 5$ mW and $P_{\text{smax}} = 20$ mW. We can observe that the CTR with no collaboration is higher,

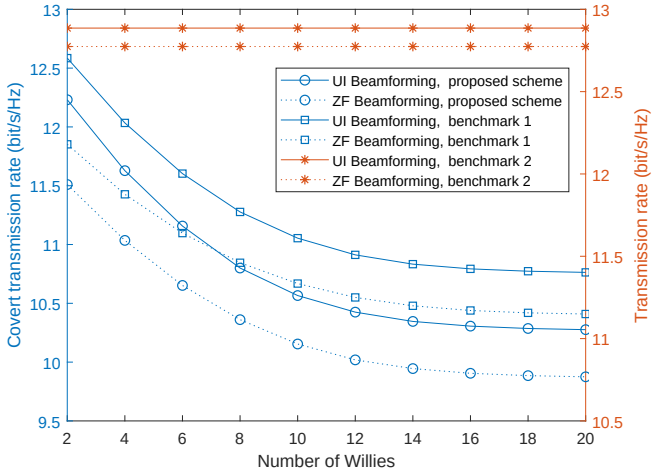

Fig. 10. Covert transmission rate and transmission rate versus number of Willies T in different benchmarks.

because it is only necessary to ensure that the minimal DOP among Willies is sufficiently high, i.e. $\min\{P_{d_t}\} \geq 1-\varepsilon, t \in \mathcal{T}$. The minimal DOP with no collaboration is higher than the GDOP with collaboration, Thus, the covertness constraint with no collaboration is relaxed, which favours the CTR. In addition, CTR will always decrease with T in both collusive and non-collusive cases.

Fig. 10 presents the CTRs achieved by the proposed scheme and benchmark 1, and also shows the transmission rate achieved by benchmark 2 with $P_{\text{cmax}} = 5$ mW and $P_{\text{smax}} = 20$ mW. There is no sensing constraint (48b) in benchmark 1, and no covertness constraint (48c) in benchmark 2, respectively. It is evident that the transmission rate in benchmark 2 surpasses the CTRs, and remains constant with respect to T. This is attributed to the removal of covertness constraint, which eliminates the need for trade-off between communication performance and covertness. Consequently, Alice can increase power, thereby significantly improving the transmission rate. In addition, benchmark 1 achieves a higher CTR compared to the proposed scheme, which stems from

the fact that Alice can gain more freedom in power allocation by removing the sensing constraint. The freedom allows for more flexible adjustment of transmission parameters according to channel conditions, thus improving the CTR. Moreover, the CTR achieved by benchmark 1 decreases as T increases, indicating that the covertness constraint can severely impact communication performance, particularly as the number of wardens increases. A comparative analysis of these three schemes provides deeper insights into the complexities and trade-off in balancing covertness, sensing, and communication.

VI. Conclusion

In this paper, we have investigated the covert ISAC of a dual-functional transmitter against multiple randomly distributed wardens. MI and CTR are adopted as the metrics of detection and covertness, respectively. The detection performance of each Willie is analyzed and the optimal detection thresholds are derived to achieve the minimal GDOP. Under this worst situation, we jointly optimize the communication and sensing beamformings to maximize the CTR while ensuring the covertness and effective sensing. Hence, a non-convex optimization problem is formulated, and UI and ZF beamformings are leveraged to address it, respectively. Simulation results demonstrate that the theoretical results are perfectly consistent with the simulated ones, and the UI beamforming outperforms the ZF beamforming in achieving the optimal trade-off among the covertness, communication and sensing, despite its higher complexity.

Appendix A
Proof of Proposition 1

According to the definition of CDF as

$$\mathcal{F}_X(x) = \Pr\{X \le x\}, \tag{91}$$

we can reformulate (27) as

$$p_{d_t}(\xi_t) = 1 - \left(\mathcal{F}_{S_{w_{ts}}}(\xi_t) - \mathcal{F}_{S_{w_{ts}}+S_{w_{tc}}}(\xi_t)\right). \tag{92}$$

Due to $h_{a_m w_t} \sim \mathcal{CN}(0,1)$, we can conclude that $|\mathbf{h}_{aw_t}\mathbf{u}_c|^2$ and $|\mathbf{h}_{aw_t}\mathbf{u}_s|^2$ both follow an exponential distribution, indicating

$$S_{w_{tc}} \sim \exp\left(\frac{r_{aw_t}^{\alpha_g}}{\rho_0 P_{ac}}\right) = \exp(a_{tc}), \tag{93}$$

and

$$S_{w_{ts}} \sim \exp\left(\frac{r_{aw_t}^{\alpha_g}}{\rho_0 P_{as}}\right) = \exp(a_{ts}). \tag{94}$$

Based on (93), the PDF of $S_{w_{ts}}$ can be expressed as

$$f_{S_{w_{ts}}}(x) = a_{ts} e^{-a_{ts}x}, x > 0, \tag{95}$$

and accordingly, the CDF of $S_{w_{ts}}$ can be calculated as

$$\mathcal{F}_{S_{w_{ts}}}(\xi_t) = 1 - e^{-a_{ts}\xi_t}. \tag{96}$$

Similarly, the PDF of $S_{w_{tc}}$ can be described as

$$f_{S_{w_{tc}}}(y) = a_{tc} e^{-a_{tc}y}, y > 0. \tag{97}$$

According to (95) and (97), the CDF of $S_{w_{ts}} + S_{w_{tc}}$ can be calculated as

$$\begin{aligned}
\mathcal{F}_{S_{w_{ts}}+S_{w_{tc}}}(\xi_t) &= \int_0^{\xi_t}\int_0^{-x+\xi_t} f_{S_{w_{ts}}}(x) f_{S_{w_{tc}}}(y) dy dx \\
&= \int_0^{\xi_t}\int_0^{-x+\xi_t} a_{ts} e^{-a_{ts}x} a_{tc} e^{-a_{tc}y} dy dx \\
&= \int_0^{\xi_t} a_{ts} e^{-a_{ts}x}\left(e^0 - e^{-a_{tc}(-x+\xi_t)}\right) dx \\
&= \int_0^{\xi_t} a_{ts} e^{-a_{ts}x} dx - \int_0^{\xi_t} a_{ts} e^{-a_{tc}\xi_t} e^{(a_{tc}-a_{ts})x} dx.
\end{aligned} \tag{98}$$

When $a_{tc} = a_{ts}$, (98) can be formulated as

$$\begin{aligned}
\mathcal{F}_{S_{w_{ts}}+S_{w_{tc}}}(\xi_t) &= \int_0^{\xi_t} a_{ts} e^{-a_{ts}x} dx - \int_0^{\xi_t} a_{ts} e^{-a_{tc}\xi_t} dx \\
&= (-e^{-a_{ts}x})|_0^{\xi_t} - \xi_t a_{ts} e^{-a_{tc}\xi_t} \\
&= 1 - e^{-a_{ts}\xi_t} - \xi_t a_{ts} e^{-a_{tc}\xi_t},
\end{aligned} \tag{99}$$

and with $a_{tc} \ne a_{ts}$, (98) can be re-expressed as

$$\begin{aligned}
\mathcal{F}_{S_{w_{ts}}+S_{w_{tc}}}(\xi_t) &= (-e^{-a_{ts}x})|_0^{\xi_t} \\
&\quad - a_{ts} e^{-a_{tc}\xi_t} \left.\frac{e^{(a_{tc}-a_{ts})x}}{a_{tc}-a_{ts}}\right|_0^{\xi_t} \\
&= -e^{-a_{ts}\xi_t} + e^0 - \frac{a_{ts}e^{-a_{ts}\xi_t}}{a_{tc}-a_{ts}} + \frac{a_{ts}e^{-a_{tc}\xi_t}}{a_{tc}-a_{ts}} \\
&= 1 - \frac{a_{ts}e^{-a_{ts}\xi_t} - a_{ts}e^{-a_{tc}\xi_t} + (a_{tc}-a_{ts})\, e^{-a_{ts}\xi_t}}{a_{tc}-a_{ts}} \\
&= 1 - \frac{a_{tc}e^{-a_{ts}\xi_t} - a_{ts}e^{-a_{tc}\xi_t}}{a_{tc}-a_{ts}}.
\end{aligned} \tag{100}$$

Combining (99) and (100), we can obtain a closed-form expression for $\mathcal{F}_{S_{w_{ts}}+S_{w_{tc}}}(\xi_t)$ as

$$\mathcal{F}_{S_{w_{ts}}+S_{w_{tc}}}(\xi_t) = \begin{cases} 1 - \dfrac{a_{tc}e^{a_{ts}} - a_{ts}e^{a_{tc}}}{(a_{tc}-a_{ts})\, e^{\xi_t}}, & a_{tc} \ne a_{ts}, \\ 1 - (1 + a_{tc}\xi_t)e^{-a_{tc}\xi_t}, & a_{tc} = a_{ts}. \end{cases} \tag{101}$$

Finally, the expression in (28) can be derived by substituting (101) and (96) into (92), and Proposition 1 is proved.

Appendix B
Proof of Proposition 3

It is difficult to analyze the monotonicity of p_e with respect to ξ_t through (31), and we need to take additional analysis. First, we calculate the first-order derivative of p_e with respect to ξ_t as

$$p_e^{'}(\xi_t) = \frac{Tp_e 2\pi \int_0^D p_{d_t}^{'}(\xi_t) \frac{r}{\pi D^2} dr}{2\pi \int_0^D p_{d_t} \frac{r}{\pi D^2} dr}, \tag{102}$$

where

$$p_{d_t}^{'}(\xi_t) = \begin{cases} -\dfrac{a_{ts}\left(a_{tc}e^{a_{tc}} - a_{ts}e^{a_{ts}}\right)}{(a_{tc}-a_{ts})\, e^{\xi_t}}, & a_{tc} \ne a_{ts}, \\ -(1 - a_{tc}\xi_t)\, a_{tc} e^{-a_{tc}\xi_t}, & a_{tc} = a_{ts}. \end{cases} \tag{103}$$

We can conclude that the negativeness or positiveness of $p_e^{'}(\xi_t)$ depends on $p_{d_t}^{'}(\xi_t)$. Due to its complexity, we delve into (103) to further analyze the monotonicity of p_e with respect to ξ_t.

(1) $a_{t_1} \neq a_{t_0}$: The zero point of $p_{d_t}^{'}(\xi_t)$ can be calculated as

$$\xi_{t0} = \frac{\ln a_{ts} - \ln a_{tc}}{a_{ts} - a_{tc}}. \tag{104}$$

If $a_{tc} > a_{ts}$, we can obtain $a_{ts} - a_{tc} < 0$. When $\xi_t > \xi_{t0}$, we have

$$(a_{ts} - a_{tc})\,\xi_t < \ln a_{ts} - \ln a_{tc}, \tag{105}$$

which leads to

$$-a_{tc}\xi_t + \ln a_{tc} < -a_{ts}\xi_t + \ln a_{ts}, \tag{106}$$

and

$$a_{tc}e^{-a_{tc}\xi_t} - a_{ts}e^{-a_{ts}\xi_t} < 0, \tag{107}$$

indicating $p_{d_t}^{'}(\xi_t) > 0$.

Similarly, $a_{tc} < a_{ts}$ can result in $a_{ts} - a_{tc} > 0$, and $\xi_t > \xi_{t0}$ can lead to

$$(a_{ts} - a_{tc})\,\xi_t > \ln a_{ts} - \ln a_{tc}. \tag{108}$$

Based on (108), we can derive

$$a_{tc}e^{-a_{tc}\xi_t} - a_{ts}e^{-a_{ts}\xi_t} > 0. \tag{109}$$

Combining $a_{ts} - a_{tc} > 0$, $p_{d_t}^{'}(\xi_t) > 0$ can be obtained. To summarize, no matter whether $a_{tc} > a_{ts}$ or $a_{tc} < a_{ts}$, $p_{d_t}^{'}(\xi_t) > 0$ can be guaranteed as long as $\xi_t > \xi_{t0}$. Therefore, we can present $p_{d_t}^{'}(\xi_t)$ as

$$p_{d_t}^{'}(\xi_t) \begin{cases} < 0, & \xi_t < \xi_{t0}, \\ = 0, & \xi_t = \xi_{t0}, \\ > 0, & \xi_t > \xi_{t0}. \end{cases} \tag{110}$$

Accordingly, we can conclude that p_e first monotonically decreases when $\xi_t < \xi_{t0}$, and then monotonically increases when $\xi_t > \xi_{t0}$, indicating that $\xi_t = \xi_{t0}$ can achieve the minimum DOP with $a_{t_1} \neq a_{t_0}$.

(2) $a_{t_1} = a_{t_0}$: Similarly, we obtain the zero point of (103) in this case as

$$\xi_{t0}^{\flat} = \frac{1}{a_{tc}}. \tag{111}$$

Accordingly, we can calculate $p_{d_t}^{'}(\xi_t)$ as

$$p_{d_t}^{'}(\xi_t) \begin{cases} < 0, & \xi_t < \xi_{t0}^{\flat}, \\ = 0, & \xi_t = \xi_{t0}^{\flat}, \\ > 0, & \xi_t > \xi_{t0}^{\flat}. \end{cases} \tag{112}$$

Thus, we can find that p_e achieves its minimum value at $\xi_t = \xi_{t0}^{\flat}$ as it first monotonically decreases and then monotonically increases with $a_{tc} = a_{ts}$. In conclusion, the optimal detection threshold of the t-th Willie can be presented as (35), and Proposition 3 is proved.

REFERENCES

[1] Y. Wu, C. Xing, J. Tang, N. Zhao, X. Y. Zhang, K. K. Wong, and G. K. Karagiannidis, "Covert ISAC: Towards collusive detection," in *Proc. IEEE ICC'25*, Montreal, Canada.

[2] X. You *et al.*, "Towards 6G wireless communication networks: vision, enabling technologies, and new paradigm shifts," *Sci. China Inf. Sci.*, vol. 64, art. no. 110301, 2021.

[3] F. Liu, L. Zheng, Y. Cui, C. Masouros, A. P. Petropulu, H. Griffiths, and Y. C. Eldar, "Seventy years of radar and communications: The road from separation to integration," *IEEE Signal Process Mag.*, vol. 40, no. 5, pp. 106–121, Jul. 2023.

[4] G. Zhu, Z. Lyu, X. Jiao, P. Liu, M. Chen, J. Xu, S. Cui, and P. Zhang, "Pushing AI to wireless network edge: an overview on integrated sensing, communication, and computation towards 6G," *Sci. China Inf. Sci.*, vol. 66, art. no. 130301, 2023.

[5] L. Chen, X. Qin, Y. Chen, and N. Zhao, "Joint waveform and clustering design for coordinated multi-point DFRC systems," *IEEE Trans. Commun.*, vol. 71, no. 3, pp. 1323–1335, Mar. 2023.

[6] X. Fang, W. Feng, Y. Chen, N. Ge, and Y. Zhang, "Joint communication and sensing toward 6G: Models and potential of using MIMO," *IEEE Internet Things J.*, vol. 10, no. 5, pp. 4093–4116, Mar. 2023.

[7] C. Sturm and W. Wiesbeck, "Waveform design and signal processing aspects for fusion of wireless communications and radar sensing," *Proc. IEEE*, vol. 99, no. 7, pp. 1236–1259, Jul. 2011.

[8] A. Hassanien, M. G. Amin, E. Aboutanios, and B. Himed, "Dual-function radar communication systems: A solution to the spectrum congestion problem," *IEEE Signal Process. Mag.*, vol. 36, no. 5, pp. 115–126, Spet. 2019.

[9] F. Liu, C. Masouros, A. Li, H. Sun, and L. Hanzo, "MU-MIMO communications with MIMO radar: From Co-existence to joint transmission," *IEEE Trans. Wireless Commun.*, vol. 17, no. 4, pp. 2755–2770, Apr. 2018.

[10] Z. Lyu, G. Zhu, and J. Xu, "Joint maneuver and beamforming design for UAV-enabled integrated sensing and communication," *IEEE Trans. Wireless Commun.*, vol. 22, no. 4, pp. 2424–2440, Apr. 2023.

[11] X. Mu, Y. Liu, L. Guo, J. Lin, and L. Hanzo, "NOMA-aided joint radar and multicast-unicast communication systems," *IEEE J. Sel. Areas Commun.*, vol. 40, no. 6, pp. 1978–1992, Jun. 2022.

[12] M. Shi, X. Li, J. Liu, and S. Lv, "Constant modulus waveform design for RIS-aided ISAC system," *IEEE Trans. Veh. Technol.*, vol. 73, no. 6, pp. 8648–8659, Jun. 2024.

[13] X. Cheng, D. Duan, S. Gao, and L. Yang, "Integrated sensing and communications (ISAC) for vehicular communication networks (VCN)," *IEEE Internet Things J.*, vol. 9, pp. 23441–23451, Dec. 2022.

[14] F. Liu, Y. Cui, C. Masouros, J. Xu, T. X. Han, Y. C. Eldar, and S. Buzzi, "Integrated sensing and communications: Toward dual-functional wireless networks for 6G and beyond," *IEEE J. Sel. Areas Commun.*, vol. 40, pp. 1728–1767, Jun. 2022.

[15] Y. Cui, F. Liu, X. Jing, and J. Mu, "Integrating sensing and communications for ubiquitous IoT: Applications, trends, and challenges," *IEEE Netw.*, vol. 35, no. 5, pp. 158–167, Oct. 2021.

[16] Y.-S. Shiu, S. Y. Chang, H.-C. Wu, S. C.-H. Huang, and H.-H. Chen, "Physical layer security in wireless networks: a tutorial," *IEEE Wireless Commun.*, vol. 18, no. 2, pp. 66–74, Apr. 2011.

[17] Y. Zou, J. Zhu, X. Wang, and L. Hanzo, "A survey on wireless security: Technical challenges, recent advances, and future trends," *Proc. IEEE*, vol. 104, no. 9, pp. 1727–1765, Sept. 2016.

[18] X. Chen, J. An, Z. Xiong, C. Xing, N. Zhao, F. R. Yu, and A. Nallanathan, "Covert communications: A comprehensive survey," *IEEE Commun. Surv. Tut.*, vol. 25, no. 2, pp. 1173–1198, 2nd Quart. 2023.

[19] B. A. Bash, D. Goeckel, and D. Towsley, "Limits of reliable communication with low probability of detection on AWGN channels," *IEEE J. Sel. Areas Commun.*, vol. 31, no. 9, pp. 1921–1930, Sept. 2013.

[20] B. A. Bash, D. Goeckel, D. Towsley, and S. Guha, "Hiding information in noise: Fundamental limits of covert wireless communication," *IEEE Commun. Mag.*, vol. 53, no. 12, pp. 26–31, Dec. 2015.

[21] M. Tatar Mamaghani and Y. Hong, "Aerial intelligent reflecting surface-enabled terahertz covert communications in beyond-5G internet of things," *IEEE Internet Things J.*, vol. 9, no. 19, pp. 19012–19033, Oct. 2022.

[22] J. Wang, W. Tang, Q. Zhu, X. Li, H. Rao, and S. Li, "Covert communication with the help of relay and channel uncertainty," *IEEE Wireless Commun. Lett.*, vol. 8, no. 1, pp. 317–320, Feb. 2019.

[23] C. Wang, X. Chen, J. An, Z. Xiong, C. Xing, N. Zhao, and D. Niyato, "Covert communication assisted by UAV-IRS," *IEEE Trans. Commun.*, vol. 71, no. 1, pp. 357–369, Jan. 2023.

[24] W. Xiong, Y. Yao, X. Fu, and S. Li, "Covert communication with cognitive jammer," *IEEE Wireless Commun. Lett.*, vol. 9, no. 10, pp. 1753–1757, Oct. 2020.

[25] R. Soltani, D. Goeckel, D. Towsley, B. A. Bash, and S. Guha, "Covert wireless communication with artificial noise generation," *IEEE Trans. Wireless Commun.*, vol. 17, pp. 7252–7267, Nov. 2018.

[26] M. Forouzesh, P. Azmi, A. Kuhestani, and P. L. Yeoh, "Covert communication and secure transmission over untrusted relaying networks in the presence of multiple wardens," *IEEE Trans. Commun.*, vol. 68, no. 6, pp. 3737–3749, Jun. 2020.

[27] Y. Jiang, L. Wang, and H.-H. Chen, "Covert communications in D2D underlaying cellular networks with antenna array assisted artificial noise transmission," *IEEE Trans. Veh. Technol.*, vol. 69, no. 3, pp. 2980–2992, Mar. 2020.

[28] A. Arghavani, S. Dey, and A. Ahln, "Covert outage minimization in the presence of multiple wardens," *IEEE Trans. Signal Process.*, vol. 71, pp. 686–700, Feb. 2023.

[29] H. Mao, Y. Liu, Z. Xiao, Z. Han, and X.-G. Xia, "Joint resource allocation and 3-D deployment for multi-UAV covert communications," *IEEE Internet Things J.*, vol. 11, no. 1, pp. 559–572, Jan. 2024.

[30] H. Du, J. Kang, D. Niyato, J. Zhang, and D. I. Kim, "Reconfigurable intelligent surface-aided joint radar and covert communications: Fundamentals, optimization, and challenges," *IEEE Veh. Technol. Mag.*, vol. 17, no. 3, pp. 54–64, Sep. 2022.

[31] S. Ma, H. Sheng, R. Yang, H. Li, Y. Wu, C. Shen, N. Al-Dhahir, and S. Li, "Covert beamforming design for integrated radar sensing and communication systems," *IEEE Trans. Wireless Commun.*, vol. 22, no. 1, pp. 718–731, Jan. 2023.

[32] J. Hu, Q. Lin, S. Yan, X. Zhou, Y. Chen, and F. Shu, "Covert transmission via integrated sensing and communication systems," *IEEE Trans. Veh. Technol.*, vol. 73, no. 3, pp. 4441–4446, Mar. 2024.

[33] Y. Zhang, W. Ni, J. Wang, W. Tang, M. Jia, Y. C. Eldar, and D. Niyato, "Robust transceiver design for covert integrated sensing and communications with imperfect CSI," *IEEE Trans. Commun.*, to appear.

[34] P. Chen, F. Xiao, L. Yang, T. A. Tsiftsis, and H. Liu, "Covert beamforming design for active RIS-assisted NOMA-ISAC systems," in *Proc. IEEE Globecom'23 Workshops*, pp. 1141–1146.

[35] I. Ghosh, A. Chattopadhyay, K. V. Mishra, and A. P. Petropulu, "Multicast with multiple wardens in IRS-aided covert DFRC system," in *Proc. IEEE ICASSP'24*, pp. 12871–12875, Seoul, Korea, Apr. 2024.

[36] B. Makki and M.-S. Alouini, "End-to-End performance analysis of delay-sensitive multi-relay networks," *IEEE Commun. Lett.*, vol. 23, no. 12, pp. 2159–2163, Dec. 2019.

[37] X. Lu, W. Yang, S. Yan, L. Tao, and D. W. K. Ng, "Joint packet generation and covert communication in delay-intolerant status update systems," *IEEE Trans. Veh. Technol.*, vol. 71, no. 2, pp. 2170–2175, Feb. 2022.

[38] K. Shahzad, X. Zhou, S. Yan, J. Hu, F. Shu, and J. Li, "Achieving covert wireless communications using a full-duplex receiver," *IEEE Trans. Wireless Commun.*, vol. 17, no. 12, pp. 8517–8530, Dec. 2018.

[39] J. Wang, W. Tang, Q. Zhu, X. Li, H. Rao, and S. Li, "Covert communication with the help of relay and channel uncertainty," *IEEE Wireless Commun. Lett.*, vol. 8, no. 1, pp. 317–320, Feb. 2019.

[40] Q. Huang, Z. Song, Z. Xiong, G. Xu, N. Zhao, and D. Niyato, "Joint resource and trajectory optimization in active IRS-aided UAV relaying networks," *IEEE Trans. Wireless Commun*, vol. 23, no. 10, pp. 13082–13094, Oct. 2024.

[41] G. Zhang, Q. Wu, M. Cui, and R. Zhang, "Securing UAV communications via joint trajectory and power control," *IEEE Trans. Wireless Commun.*, vol. 18, no. 2, pp. 1376–1389, Feb. 2019.

Yujie Wu received the B.S. degree from the Dalian University of Technology, China, in 2022. She is currently pursuing the Ph.D. degree with the School of Information and Communication Engineering, Dalian University of Technology, China. Her current research interests include covert communication, intelligent reflecting surface, and integrated sensing and communication. She won the best paper award in ICC 2025.

Chengwen Xing (Member, IEEE) received the B.Eng. degree from Xidian University, Xi'an, China, in 2005, and the Ph.D. degree from the University of Hong Kong, Hong Kong, China, in 2010. Since September 2010, he has been with the School of Information and Electronics, Beijing Institute of Technology, Beijing, China, where he is currently a Full Professor. His current research interests include machine learning, statistical signal processing, convex optimization, multivariate statistics, and array signal processing.

Jie Tang (Senior Member, IEEE) received the B.Eng. degree from the South China University of Technology, China, the M.Sc. degree from the University of Bristol, U.K., and the Ph.D. degree from Loughborough University, U.K. From 2013 to 2015, he was a Research Associate at the School of Electrical and Electronic Engineering, The University of Manchester, U.K. He is currently a Professor at the School of Electronic and Information Engineering, South China University of Technology. His current research interests include SWIPT, UAV communications, ISAC and RIS. He received the IEEE ComSoc Asia-Pacific Outstanding Young Researcher Award in 2021. He was a co-recipient of Best Paper Awards at the ICNC 2018, CSPS 2018, WCSP 2019, 6GN 2020, AICON2021, ECIE2024 and ECIE2025. He also served as a Track Co-Chair for IEEE VTC-Spring 2018 and 2022, the Symposium Co-Chair for IEEE/CIC ICCC 2020, ICCT2024, ICCT2025 and IEEE ComComAp 2019, the TPC Co-Chair for EAI GreeNets 2019, and the Workshop Co-Chair for IEEE ICCC/CIC 2019. He was the Vice Chair of the Special Interest Group on Green Cellular Networks within the IEEE ComSoc Green Communications and Computing Technical Committee. He is serving as an Editor for IEEE WIRELESS COMMUNICATIONS LETTERS, IEEE SYSTEMS JOURNAL, IEEE OPEN JOURNAL OF THE COMMUNICATIONS SOCIETY and EURASIP Journal on Wireless Communications and Networking.

Nan Zhao (Senior Member, IEEE) is currently a Professor at Dalian University of Technology, China. He received the Ph.D. degree in information and communication engineering in 2011, from Harbin Institute of Technology, Harbin, China. Dr. Zhao is serving on the editorial boards of IEEE Wireless Communications and IEEE Wireless Communications Letters. He won the best paper awards in IEEE VTC 2017 Spring, ICNC 2018, WCSP 2018 and WCSP 2019. He also received the IEEE Communications Society Asia Pacific Board Outstanding Young Researcher Award in 2018.

Xiu Yin Zhang (Fellow, IEEE) received the B. S. degree in communication engineering from Chongqing University of Posts and Telecommunications, Chongqing, China, in 2001, the M.S. degree in electronic engineering from South China University of Technology, Guangzhou, China, in 2006, and the PhD degree in electronic engineering from City University of Hong Kong, Hong KongChina, in 2009.

From 2001 to 2003, he was with ZTE Corporation, Shenzhen, China. He was a Research Assistant from July 2006 to June 2007 and a Research Fellow from August 2009 to January 2010 with the City University of Hong Kong. He is currently a full professor with the School of Microelectronics, South China University of Technology. He also serves as the vice chair of IEEE Guangzhou section and the director of the Engineering Research Center of Short-Distance Wireless Communications and Network, Ministry of Education. He has authored or coauthored more than 400 internationally journal and conference papers (including more than 160 IEEE Transactions). His research interests include antennas, RFICs, RF components and sub-systems, intelligent wireless communications and sensing.

Dr. Zhang is a Fellow of IEEE, IET, CIE and CIC. He has served as General chair/Co-chair/Technical Program Committee (TPC) chair/ Co-chair for a number of conferences. He was a recipient of the National Science Foundation for Distinguished Young Scholars of China. He won the first prize of 2016 Guangdong Provincial Natural Science Award, 2021 Guangdong Provincial Technological Invention Award, and 2022 Silver Award of China Patent Award. He was the supervisor of several conference best paper award winners. He is or was an Associate Editor for IEEE TAP, AWPL, APM and OJAP.

Kai-Kit Wong (Fellow, IEEE) received the BEng, the MPhil, and the PhD degrees, all in Electrical and Electronic Engineering, from the Hong Kong University of Science and Technology, Hong Kong, in 1996, 1998, and 2001, respectively. After graduation, he took up academic and research positions at the University of Hong Kong, Lucent Technologies, Bell-Labs, Holmdel, the Smart Antennas Research Group of Stanford University, and the University of Hull, UK. He is Chair in Wireless Communications at the Department of Electronic and Electrical Engineering, University College London, UK. His current research centers around 6G and beyond mobile communications. He is Fellow of IEEE and IET. He served as the Editor-in-Chief for IEEE Wireless Communications Letters between 2020 and 2023.

George K. Karagiannidis (Fellow, IEEE) is currently Professor in the Electrical and Computer Engineering Dept. of Aristotle University of Thessaloniki, Greece and Head of Wireless Communications & Information Processing (WCIP) Group. He is also Visitor Professor at Taif University, Taif, Saudi Arabia. His research interests are in the areas of Wireless Communications Systems and Networks, Signal processing, Optical Wireless Communications, Wireless Power Transfer and Applications and Communications & Signal Processing for Biomedical Engineering. Dr. Karagiannidis is the Editor-in Chief of IEEE Transactions on Communications and in the past was the Editor-in Chief of IEEE Communications Letters. Recently, he received three prestigious awards: The 2021 IEEE ComSoc RCC Technical Recognition Award, the 2018 IEEE ComSoc SPCE Technical Recognition Award and the 2022 Humboldt Research Award from Alexander von Humboldt Foundation. Dr. Karagiannidis is one of the highly-cited authors across all areas of Electrical Engineering, recognized from Clarivate Analytics as Web-of-Science Highly-Cited Researcher in the 10 consecutive years 2015-2024.